Comparative study of DC/DC electric vehicle charging system with conventional transformer and planar transformer

MACIEJ RUDAWSKI ⊠, KAROL FATYGA, ŁUKASZ KWAŚNY

Lublin University of Technology
ul. Nadbystrzycka 38d, 20-618 Lublin, Poland
e-mail: { ⊠m.rudawski/k.fatyga/ l.kwasny}@pollub.pl

Abstract: This paper presents an analysis of electric vehicle charging station operation based on a dual active bridge topology. Two cases are considered: one with the use of a medium frequency planar transformer, the other with a conventional Litz winding transformer. An analysis was performed using both solutions in order to compare the performance characteristics of the system for both cases and to present the differences between each transformer solution. The analysis was based on tests carried out on the full-scale model of an electric vehicle charging station, which is the result of the project "Electric vehicle charging system integrated with lighting infrastructure" realized by the Department of Drives and Electrical Machines, Lublin University of Technology. The results presented in the paper show that the conventional transformer used in the research achieved better results than the planar transformer. Based on the results obtained, the validity of using both solutions in electric vehicle charging stations was considered.

Key words: conventional transformer, dual active bridge, electric vehicle charging station, planar transformer

1. Introduction

The increasing problem of climate change, caused by the level of greenhouse gas emissions into the atmosphere, is provoking a popularisation of electric vehicles on the market. The state of the currently existing power transmission and distribution infrastructure requires continuous adaptation to this trend. The key goal of this development is to ensure adequate availability of

electric vehicle charging stations to enable the most effective transfer of energy from the distribution network to the batteries and energy transfer in the opposite direction to achieve greater flexibility of the power system. Considering that a single charging station may have a power consumption in the range of 50 kW–450 kW, the operation of a significantly large EV charging infrastructure in the power grid will place a significant load on the power system [1–3]. This means that the parameters of charging station performance, such as the efficiency or the level of electromagnetic interference generated and injected into the grid, will have a great impact on the operation of the entire system. This indicates the need to develop the technology of bidirectional charging stations with technologically advanced solutions characterized by high efficiency and high reliability. This publication presents a study of the converter system of an electric vehicle charging station that is the result of the project "Electric vehicle charging system integrated with lighting infrastructure". The tests were carried out on two types of medium-frequency transformers, namely a planar transformer and a conventional transformer. The conventional transformer was a construction with a three-column ferrite core with windings made of Litz wire wound on the central column. Both transformers were designed and manufactured for the purpose of the project as short series prototype units. The aim of the research is to present the performance characteristics and to compare the efficiency achieved by the system for both types of transformers. To achieve this goal, both transformers were purposefully designed, with calculations based on works [4, 5], which present methods for the design of medium frequency transformers with Litz winding for applications in voltage converters, which require high efficiency.

Fig. 1. View of electric vehicle charging statnion under study

The other competitive approach is the use of similar transformers with a conventional magnetic circuit structure but with planar windings [6, 7]. As in planar transformers, the use of these windings results in an increase in parasitic capacitances. Publication [8] describes a method for designing a planar transformer with reduced parasitic capacitance, which can lead to reduced voltage and current oscillations in the transformer waveforms. Paper [9] presents a unidirectional

vehicle charging station based on a transformer with tap windings. The paper also addresses the problem of current and voltage oscillations occurring in a planar transformer. There are some publications that investigate this issue and present methods to mitigate this problem. Work [10] presents the influence of the slew rate change in the rising and falling edge of the voltage of a transformer on the level of generated oscillations and indicates how to reduce them by changing the voltage slope. In publication [11], the authors also point out the influence of low transformer impedance at high frequencies, and propose an extended method for modelling transformers that allows obtaining accurate simulation results. They also point out the link between the oscillations occurring in the transformer and the level of generated electromagnetic interference. An important aspect to consider when designing a transformer for a DC/DC converter is its thermal properties. Appropriate analysis of the temperature distribution makes it possible to eliminate overheating of the transformer and to eliminate, for example, the thermal stresses [12, 13] inside the core, significantly extending its operational lifespan. There are many works focusing on the mathematical modelling of thermal properties for planar transformers. Publication [14] presents a model of the thermal properties of a planar transformer, while publication [15] presents a non-linear mathematical model for a planar transformer. In the case of paper [16], the authors present a method for determining power losses using a thermal imaging camera. For conventional transformers, in publication [17], the authors propose the use of 3D analysis in a high-frequency transformer. In publication [18], a numerical analysis of a push-pull transformer is presented. Works [19] and [20] present thermal models used in the design process of a transformer for a dc/dc converter. Throughout the analysis, the selected shape of windings is the determining factor, paper [21] presents methods for optimising the winding size depending on the winding shape used. Another solution attempted in the literature is a non-isolated converter. The paper [22] presents a soft-switched non-isolated high step-up multi-port DC-DC converter for a hybrid energy system. Publication [23] presents a non-isolated converter for applications in microgrids or photovoltaic farms. Similarly, publication [24] proposes the design of a non-isolated converter for applications in cooperation with renewable energy sources providing at the same time a high voltage gain. In this paper, due to the intention to avoid problems occurring in non-isolated inverter designs, such as the existence of common-mode interference, and due to the aim of increased safety of the overall device, the focus is on isolated inverters. This article is divided into six chapters. The first chapter is an introduction outlining the current state of the art of the subject under study. In the second chapter, typical topologies of electric vehicle charging stations for unidirectional and bidirectional energy transfer are presented. Construction differences and comparison of properties of both solutions are described. The third chapter describes the properties of transformers used during the research. It compares both solutions in terms of construction and an electrical equivalent diagram. The fourth chapter presents a test bench in the form of an electric vehicle charging module, which is the result of the project. The fifth chapter contains the results of tests carried out for both cases and conclusions drawn on their basis. The last chapter contains a conclusion of the entire work. Efficiency curves and a comparison of primary and secondary voltage waveforms, as well as the current flowing through the transformer are presented. High-frequency oscillations present in the waveforms of the planar transformer and a method of eliminating these disturbances to the conventional transformer level, as well as the influence of these changes on the system operation, are highlighted.

2. Structure of electric vehicle charging stations

In the structure of electric vehicle charging stations, a distinction may be made between designs ensuring unidirectional and bidirectional energy flow. The first category includes the stations with the PSFB (Phase Shift Full Bridge) output stage [25–29] in which the energy is transferred only unidirectionally from the utility grid to the electric vehicle. In this design, the rectifier and one of the bridges of the DC/DC converter are made of non-controlled elements.
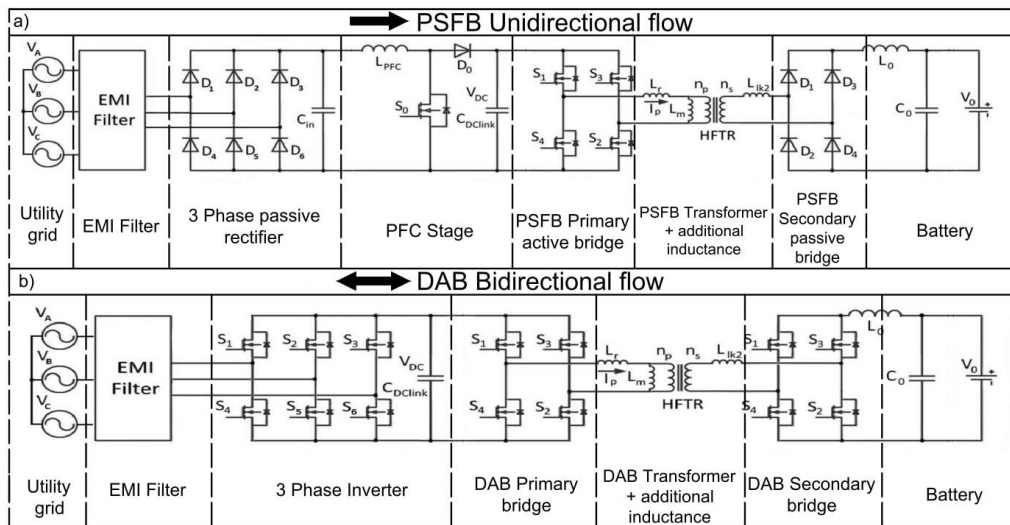

Fig. 2. Diagram of an electric vehicle charging station: (a) one-way PSFB; (b) two-way DAB

Only one bridge of the DC/DC converter and the PFC (Power Factor Correction) circuit are controllable [30,31]. The use of more non-controllable elements translates into lower complexity of the whole system and a simpler control system, which also reduces the cost. The other category of electric vehicle charging stations includes the station based on the Dual Active Bridge DAB converter [4, 29, 32, 34]. Such a system enables bidirectional energy transfer, which gives wider possibilities of optimising the operation of the entire utility grid [32]. All semiconductor elements in this circuit are fully controllable. The bridge rectifier in this case also acts as a grid inverter for energy transfer from the electric vehicle to the grid.

Due to the full controllability, no power factor correction system is required. It means higher control complexity and manufacturing costs, but it also increases the opportunities for optimising operation due to the possibilities offered by a bidirectional power transfer, such as V2G functionality (Vehicle 2 Grid) [2, 33]. From the grid perspective, this translates into significant cost reduction during operation [32]. A comparison of the two designs is shown in Tables 1 and 2. They show the results obtained for the device under study. The values obtained for the PSFB topology were obtained in the initial phase of the experiments when the presented design was still under consideration. Tables 1 and 2 show the results for the same power as for the DAB circuit.

Table 1. Comparison of the AC/DC stage parameters of PSFB and DAB stations

AC/DC stage		
	PSFB	**DAB**
No. of controllable elements	1	6
No. of measurements	$2 \times V, 1 \times I$	$4 \times V, 3 \times I$
Required algorithm	No	Yes
Power factor correction	Required	Embedded
THD (80%P)	3.1%	1.2%
Efficiency	95.5%	97%
Power factor adjustment	No	From $\cos \varphi = -0.5$ to $\cos \varphi = 0.5$
Bidirectionality	No	Yes

Table 2. Comparison of the AC/DC stage parameters of PSFB and DAB stations

DC/DC stage		
	PSFB	**DAB**
No. of controllable elements	4	8
No. of measurements	$2 \times V, 1 \times I$	$2 \times V, 1 \times I$
Required algorithm	Yes	Yes
Efficiency	96.5%	98%
Bidirectionality	No	Yes
Voltage gain factor	limited by DC bus voltage and transformer ratio	limited by voltage class of semiconductors

3. Comparison of transformers for charging stations

In power conversion systems, transformer design has a fundamental impact on the efficiency of the overall system. In medium and high frequency applications, phenomena such as skin effect or proximity effect, which cause the current not to flow through the entire cross-section of the winding and consequently increase the resistance of the windings, become a key problem.

This requires a different design approach. One of the currently used solutions are planar transformers, which utilize flat windings, usually in the form of multilayer printed circuits [35]. The large width-to-height ratio of the winding allows for a significant reduction of the skin effect.

Unfortunately, the large surface area of these windings makes planar transformers to be characterised by larger inter-winding capacitances than conventional transformers. This results in resonant circuits with frequencies of the order of megahertz, visible in the voltage and current
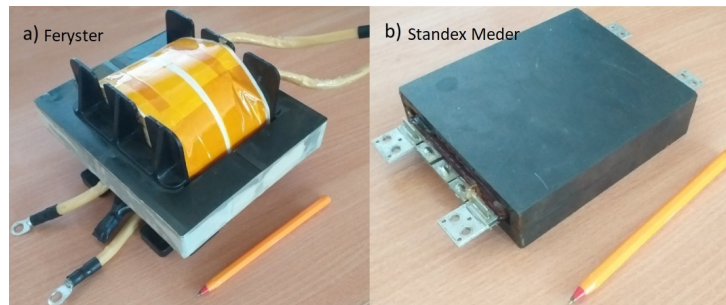
Fig. 3. Transformers examined: (a) conventional Feryster transformer; (b) Standex Meder planar transformer
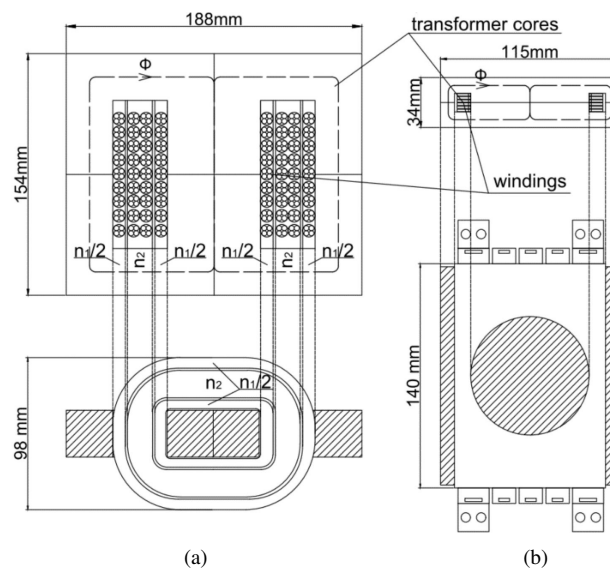

Fig. 4. Cross-section of a planar and a conventional transformer

waveforms of the transformer [10]. The amplitude of these oscillations can reach in value the amplitude of the control waveform.

The occurring oscillations have a negative effect on the level of electromagnetic interference generated by the system [11]. In order to bring these oscillations down to the level comparable to a conventional transformer, an additional leakage inductance can be used on the primary and secondary sides of the planar transformer when operating the system. This case is presented later in the publication. The windings used in the planar transformer allow the design of more compact structures. It also allows the transformer to be placed directly within the PCB of the entire system. However, the disadvantage of this solution is the high manufacturing cost of multi-layer PCBs. The parallel connection of the windings often used in planar transformers contributes to an increase in skin effect and proximity effect, reducing the benefits of using flat windings.

The conventional transformer under study was designed for use in an electric vehicle charging station. The windings were made as a parallel connection of four Litz wires in a layer winding. The first layer consists of half of the primary side winding, on which the secondary winding is wound. The third layer consists of the second half of the primary winding. The individual layers have been offset from each other in order to increase the leakage inductance.

The use of a Litz conductor allows one to reduce the skin effect by dividing the flowing current into many conductors with a small cross-section. The parameters of the tested transformers are shown in Table 3. Based on the measurements, the parameters of the equivalent diagram both transformers were determined. The equivalent circuit is shown in Fig. 5, and the measured parameters are presented in Table 4. The flat windings used in the construction of the planar

Table 3. Comparison of the DC/DC stage of the station with the PSFB and DAB stages

| Transformer	Planar	Conventional
Design power	50 kW	36.8 kW
Design frequency	100 KHz	45 kHz
Secondary side voltage	650 V	520 V
Secondary side current	77 A	80 A
Core material	3C94	3C94
Core height	3.4 mm	3.2 mm
Core width	11.5 mm	15.4 mm
Core length	14 mm	18.8 mm
Column width	76 mm	56 mm
Transformer height	3.4 mm	12.5 mm
Transformer width	11.5 mm	15.4 mm
Transformer length	20 mm	18.8 mm
No. of primary side windings	4	18
No. of secondary side windings	4	22
Shape of windings	flat windings	$4 \times$ Litz
Power density	33 kW/kg	15 kW/kg
Magnetic path length	149 mm	350 mm
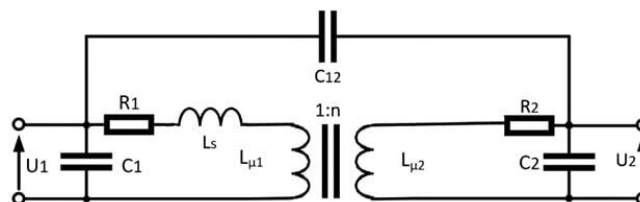
Fig. 5. Equivalent diagram of a transformer

transformer create considerable capacitance due to their surface area, which is one of the reasons for the occurrence of high-frequency oscillations in voltage and current waveforms [10, 11]. The planar transformer is characterised by winding capacitances C_1 and C_2, being an order of magnitude higher than in a conventional transformer, and the leakage inductance L_s of the order of magnitude lower than in the conventional transformer. This results directly from the constructional characteristics of the planar transformer.

Table 4. Equivalent diagram parameters of tested transformers

	Transformer	
	Planar	**Conventional**
R_1	0.1 Ω	0.2 Ω
R_2	0.1 Ω	0.3 Ω
L_s	0.7 μH	4.9 μH
$L_{\mu 1}$	575 μH	475.8 μH
$L_{\mu 2}$	575 μH	334.7 μH
C_{12}	362 pF	273 pF
C_1	397 pF	496 nF
C_2	397 pF	661 nF
n	1 : 1	1 : 1.2

4. Test stand

Figure 6 shows the inside of the test charging module used for the study. The figure shows a model of a bidirectional electric vehicle charging station based on a DAB converter. The DC bus contains capacitors with a capacitance of 750 μF each. The H-bridges shown in the figure are built with silicon carbide MOSFET power transistors. The bridges were also supplied with additional 3×22 μF capacitors. The operating frequency of the inverter was 100 kHz. The tests were performed for the same power consumed at the secondary side with the assumption of unidirectional power flow, simulating the case of vehicle battery charging. The secondary side power was tested in the range from 0.0 kW to 7.3 kW.

Three operating cases of the system were studied:
- with a conventional transformer installed with an additional dissipation inductance on the primary side equal to $L_s = 4.2$ μH,
- with a planar transformer with an additional dissipation inductance at the primary side equal to $L_s = 4.2$ μH,
- with the planar transformer installed with additional dispersion inductance divided on both sides of the transformer $L_{s1} = L_{s2} = 2.1$ μH.

In order to obtain the same power, tests were performed using two identical DC power supplies simulating the DC bus of the system at the input and the battery of the electric vehicle at the output. The schematic diagram of the tested DAB converter is shown in Fig. 7. The mathematical model of
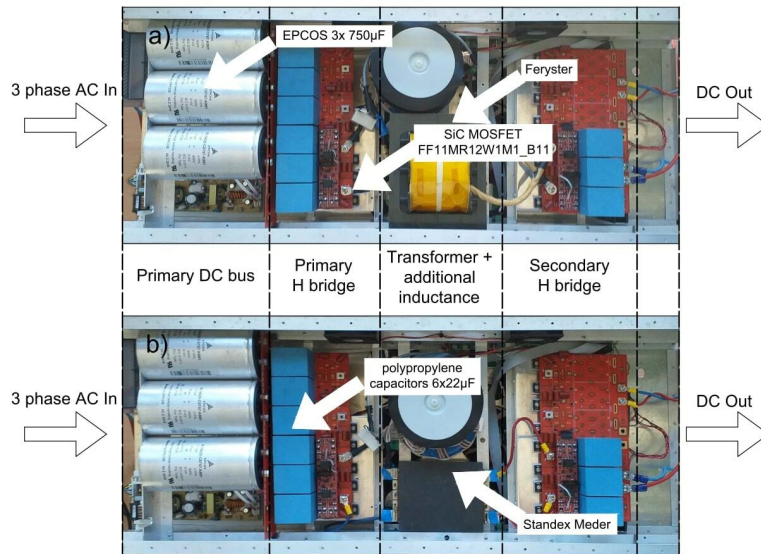
Fig. 6. View of tested system

the system under study was determined on the basis of the publications [32, 36–38] where precise mathematical relationships are presented. The power transfer between the two inverter bridges can be shown as an equivalent of two voltage sources connected together by series inductance. The voltage sources are the inverter bridges, while the inductance is the transformer leakage inductance in combination with additional series inductance.
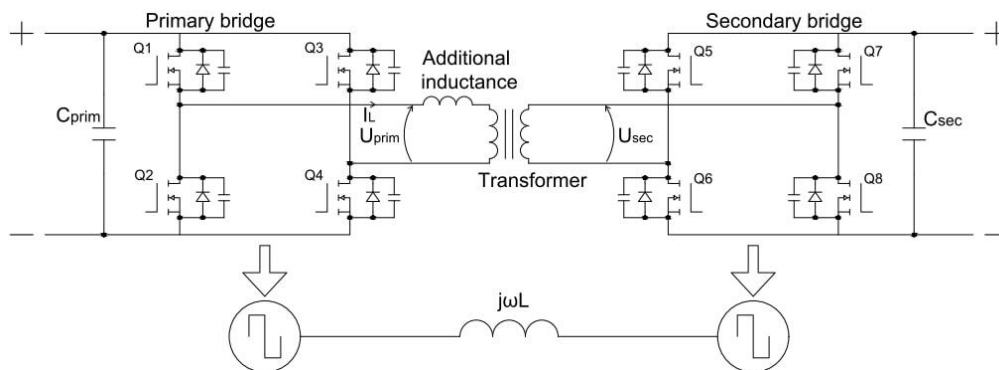

Fig. 7. Diagram of tested system

The transfer of energy takes place by changing the phase shift of the voltages generated by the bridges relative to each other. This gives an active power flow according to Eq. (1), [36].

$$P = \frac{U_{\text{prim}} U_{\text{sec}} \sin(\varphi)}{2\pi f L} ,$$ (1)

where: U_{prim} is the primary side voltage, U_{sec} is the secondary side voltage, φ is the phase shift between bridge voltages, f is the switching frequency, L is the sum of the leakage inductance and additional series inductance. The direction of the energy flow in this case takes place from the bridge, the voltage of which is leading in phase, to the bridge, the voltage of which is lagging in phase, as shown in Fig. 8, where U_{prim} represents the bridge voltage on the primary side of the transformer, U_{sec} is the bridge voltage on the secondary side of the transformer and *Il* is the current flowing through the transformer on the primary side. The power transferred by the converter depends on the sine of the phase shift angle, which means that the maximum power transferred by the bridge occurs for the angle $\varphi = 90°$, and the relation $P = f(\varphi)$ is non-linear.
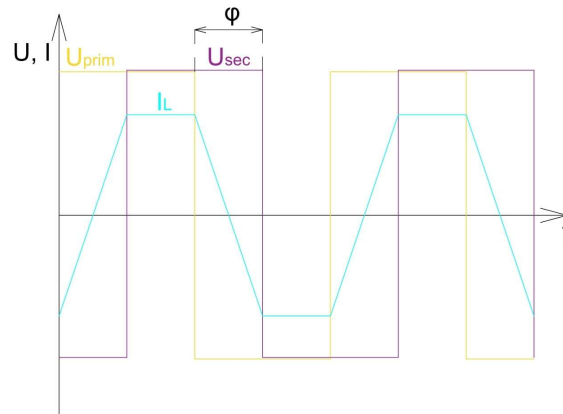

Fig. 8. The voltage and current waveforms of the system under test

If we add to Formula (1) the transformer ratio and eliminate the dependence of the sine of the angle, we obtain [37]:

$$P = \frac{nU_{\text{prim}}U_{\text{sec}}\varphi(\pi - \varphi)}{2\pi^2 f L} \ . \tag{2}$$

From this formula we can extract the relationship for the required phase shift between the bridge voltages to achieve the assumed power flow:

$$\varphi = \frac{\pi}{2} \times \left(1 - \sqrt{1 - \frac{8 f L P}{nU_{\text{prim}}U_{\text{sec}}}}\right) . \tag{3}$$

From these relationships we are able to obtain the required power flow in the system.

5. Experimental and analytical results

The tests were carried out for loads from 0.0 kW to 7.3 kW. Figure 9 shows the obtained system efficiencies of the tested dual active bridge inverter. The most important results are presented in Table 5. The highest efficiency obtained was 98.6% for the load equal to $P = 1.5$ kW obtained on a conventional transformer. The corresponding efficiency for the planar transformer

was $\eta = 97\%$ for the case without split additional inductance and $\eta = 97.9\%$ for the case with split additional inductance. In the studied system, the conventional transformer achieved slightly better efficiencies over the entire power flow range, obtaining efficiency differences for low loads $P = 1.5$ kW equal to $\Delta\eta = 1.6\%$ and for high loads $P = 7.7$ kW equal to $\Delta\eta = 0.9\%$. The planar transformer with split inductance achieved slightly better efficiencies with differences from the conventional transformer of $\Delta\eta = 0.7\%$ for $P = 1.5$ kW and $\Delta\eta = 1.2\%$ for $P = 7.3$ kW. These results show that in a long-term operation, using split inductance will result in significant energy savings. This shows that with the right design approach, in specific applications, it is possible to make a conventional transformer with efficiencies close to or even higher than a planar transformer.
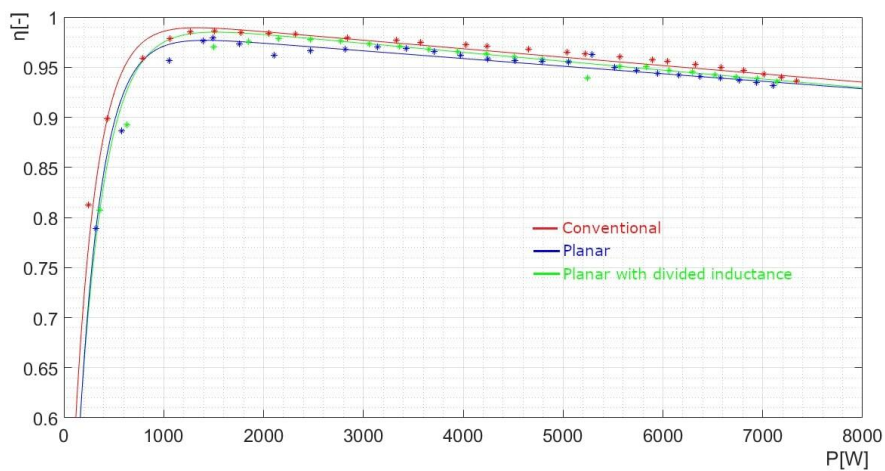

Fig. 9. Efficiency characteristics obtained

Table 5. Summary of selected measurement results

	Transformer		
	Conventional	**Planar**	**Planar divided inductance**
	η [–]	η [–]	η [–]
$P = 50$ W	0.463	0.455	0.377
$P = 1500$ W	0.986	0.97	0.979
$P = 4000$ W	0.972	0.966	0.962
$P = 6000$ W	0.956	0.947	0.944
$P = 7300$ W	0.94	0.934	0.915

Using a conventional transformer also eliminates a number of problems that can be encountered when working with planar transformers.

One such problem observed in the system under study is the occurrence of high current and voltage oscillations of the transformer as shown in Fig. 10, which results in increased EMI generation and system efficiency decrease [11]. These are a result of the resonance created between the transformer capacitances and the PCB power path inductance. One of the ways of limiting this phenomenon is to use an additional leakage inductance on both sides of the transformer. In this case, the oscillations are reduced as shown in Fig. 1, but they are still higher than in the conventional transformer shown in Fig. 12. The thermal images presented in Fig. 13 show that the elements emitting the most heat are the transformer, additional inductors and
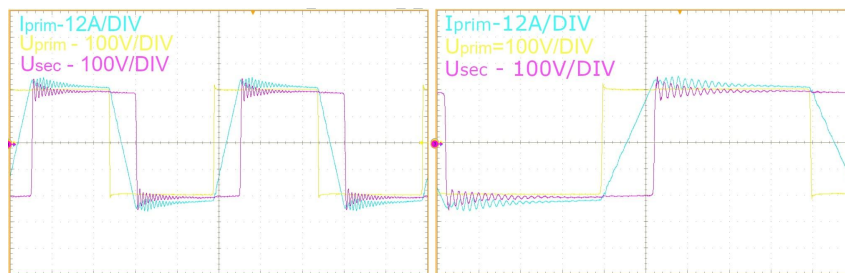
Fig. 10. Voltage and current waveforms on the primary and secondary side in the planar transformer circuit for phase shift $\varphi = 45°$
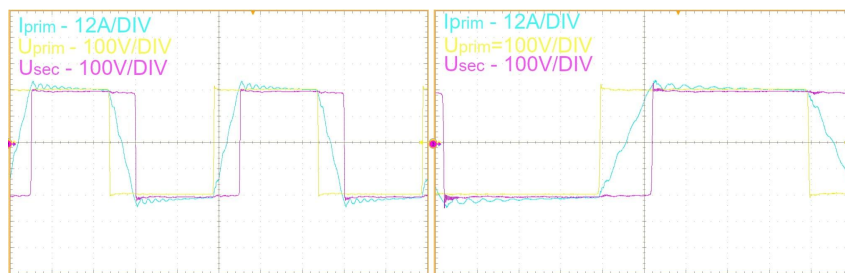

Fig. 11. Voltage and current waveforms on the primary and secondary side in the planar transformer circuit with divided additional inductance for phase shift $\varphi = 45°$
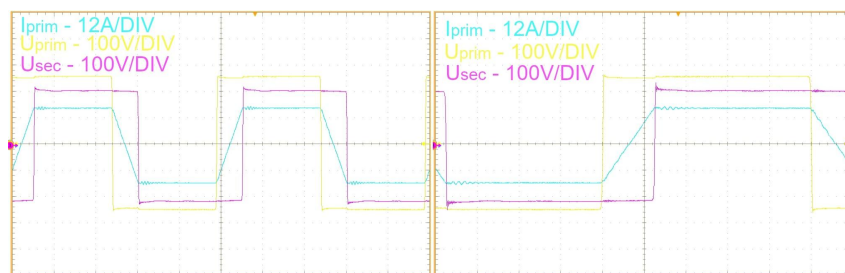

Fig. 12. Voltage and current waveforms on the primary and secondary side in the conventional transformer circuit for phase shift $\varphi = 45°$

transistor drivers. The planar transformer was placed in a harness made of aluminium according to the manufacturer's recommendations, which was removed for temperature measurement. The temperature distribution allows us to conclude that most of the system losses occur on these components, especially on the transformer, due to the additional inductance resulting from their size. For the planar transformer case, the additional inductances and the transformer itself reached higher temperatures than in the conventional transformer case. In the case of the conventional transformer, only the windings heated up, the core remained close to ambient temperature, while in the planar transformer, the core reached higher temperatures. This is due to the difference in the number of windings of the two transformers. Due to the small number of windings in the planar transformer, the electromagnetic flux density in the core reaches high values, resulting in high Eddy current losses in the core when operating at 100 kHz.
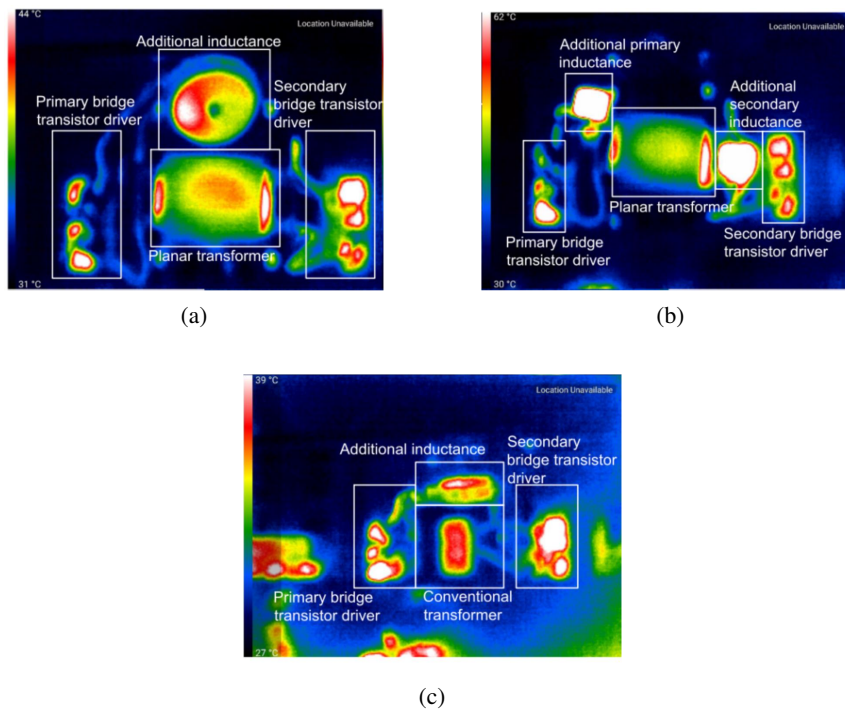

(a)

(b)

(c)

Fig. 13. Thermal images on 7.3 kW load for: (a) planar transformer; (b) planar transformer with divided additional inductance; (c) conventional transformer

For example, the manufacturer of the material used specifies the level of active losses in the core as 100 kW/m^3 for an induction of 100 mT.

In the case of a conventional transformer, the higher number of windings resulted in lower losses in the core, but higher resistive losses in the windings. Figure 14 shows the results of a charge and discharge test carried out on a real BMW I3 electric vehicle. Power was varied in steps allowing time for the system to stabilise. In the first phase, an initial test run was carried out, followed by a test of bidirectional energy transfer, by charging and discharging the battery of

the electric vehicle. As can be seen from the graph presented, the system allows dynamic control of power flow in cooperation with the real device.
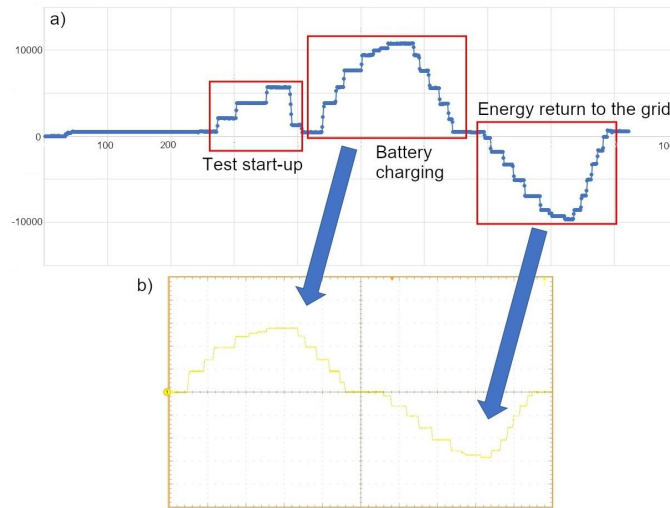

Fig. 14. Input power (a) and output current waveforms (b) of the charging system

6. Conclusions

The used bidirectional converter topology appears to be the most promising for EV charging station applications due to current trends of using EVs as mobile energy storage in cooperation with technologies such as G2V or virtual prosumers. The use of an isolated topology eliminates common-mode interference problems and increases the safety of the entire solution, which simplifies the implementation of the entire device into widespread use. The results obtained show that in specific applications it is possible to obtain a conventional transformer design with efficiency close to or higher than a planar transformer. For the case studied, a slightly higher efficiency was achieved for the conventional transformer. The use of a conventional transformer removed the need of eliminating the phenomena of current and voltage oscillations. Prototyping of conventional transformers is cheaper, more available and possible to implement within the country. At this moment, a significant amount of technology related to planar transformers is controlled by a very narrow group of manufacturers. The disadvantages of using a conventional transformer are its larger size and lower power density. However, planar transformers often require additional harnesses to improve the cooling conditions of the core and its mechanical strength, which reduces the size advantage over a conventional transformer. Mechanical durability is important in the context of long-term work in atmospheric conditions, where the system is exposed to constant temperature changes. Planar transformer technology is relatively new and still needs a lot of research. It has a very high potential to be introduced into widespread use, but at this point, taking into account the results obtained and the observations made on the performance of the system in the indicated cases, the use of conventional transformers in many solutions is deeply justified.

References

[1] Zaferanlouei S., Zecchino A., Farahmand H., *Impact of large-scale EV integration and fast chargers in a Norwegian LV grid*, The Journal of Engineering (2019), DOI: 10.1049/joe.2018.9318.

[2] Khan M.M.H., Hossain A., Ullah A., Hossain Lipu M.S., Siddiquee S.M.S., Alam M.S., Jamal T., Ahmed H., *Integration of Large-Scale Electric Vehicles into Utility Grid: An Efficient Approach for Impact Analysis and Power Quality Assessment*, Sustainability, vol. 13, 10943 (2021), DOI: 10.3390/su131910943.

[3] Knezović K., Marinelli M., Zecchino A., Andersen P., Traeholt C., *Supporting involvement of electric vehicles in distribution grids: Lowering the barriers for a proactive integration*, Energy, vol. 134, pp. 458–468 (2017), DOI: 10.1016/j.energy.2017.06.075.

[4] Mu M., Xue L., Boroyevich D., Hughes B., Mattavelli P., *Design of integrated transformer and inductor for high frequency dual active bridge GaN Charger for PHEV*, IEEE Applied Power Electronics Conference and Exposition (APEC), pp. 579–585 (2015), DOI: 10.1109/APEC.2015.7104407.

[5] Zou S., Lu J., Mallik A., Khaligh A., *Modeling and Optimization of an Integrated Transformer for Electric Vehicle On-Board Charger Applications*, in IEEE Transactions on Transportation Electrification, vol. 4, no. 2, pp. 355–363 (2018), DOI: 10.1109/TTE.2018.2804328.

[6] Barrios E.L., Urtasun A., Ursúa A., Marroyo L., Sanchis P., *High-Frequency Power Transformers with Foil Windings: Maximum Interleaving and Optimal Design*, IEEE Transactions on Power Electronics, vol. 30, no. 10, pp. 5712–5723 (2015), DOI: 10.1109/TPEL.2014.2368832.

[7] Agarwal R., Martin S., Shi Y., Li H., *High Frequency Transformer Design for Medium Voltage Shipboard DC-DC Converter*, IEEE Electric Ship Technologies Symposium (ESTS), pp. 499–504 (2019), DOI: 10.1109/ESTS.2019.8847922.

[8] Zhang Z., Liu C., Wang M., Si Y., Liu Y., Lei Q., *High-Efficiency High-Power-Density CLLC Resonant Converter with Low-Stray-Capacitance and Well-Heat-Dissipated Planar Transformer for EV On-Board Charger*, IEEE Transactions on Power Electronics, vol. 35, no. 10, pp. 10831–10851 (2020), DOI: 10.1109/TPEL.2020.2980313.

[9] Wang H., Shang M., Shu D., *Design Considerations of Efficiency Enhanced LLC PEV Charger Using Reconfigurable Transformer*, IEEE Transactions on Vehicular Technology, vol. 68, no. 9, pp. 8642–8651 (2019), DOI: 10.1109/TVT.2019.2930551.

[10] Cui B., Xue P., Jiang X., *Elimination of High Frequency Oscillation in Dual Active Bridge Converters by dv/dt Optimization*, IEEE Access, vol. 7, pp. 55554–55564 (2019), DOI: 10.1109/ACCESS.2019.2910597.

[11] Qin Z., Shen Z., Blaabjerg F., Bauer P., *Transformer Current Ringing in Dual Active Bridge Converters*, in IEEE Transactions on Industrial Electronics, vol. 68, no. 12, pp. 12130–12140 (2021), DOI: 10.1109/TIE.2020.3040681.

[12] Ropoteanu C., Codreanu N., Ionescu C., *Thermal investigation of a planar core power transformer*, 39th International Spring Seminar on Electronics Technology (ISSE) (2016), DOI: 10.1109/ISSE.2016.7563171.

[13] Loyaua V., Lo Bue M., Mazaleyrat F., *Measurement of magnetic losses by thermal method applied to power ferrites at high level of induction and frequency*, Review of Scientific Instruments (2009), DOI: 10.1063/1.3079382.

[14] Górski K., Górecki K., *Modelling thermal properties of planar transformers*, Przegląd Elektrotechniczny (2017), DOI: 10.15199/48.2017.02.45.

[15] Górski K., Górecki K., *Non-linear thermal model of planar transformers*, 21st European Microelectronics and Packaging Conference (EMPC) & Exhibition (2017), DOI: 10.23919/EMPC.2017.8346913.

[16] Barlik R., Nowak M., Grzejszczak P., Zdanowski M., *Estimation of power losses in a high-frequency planar transformer using a thermal camera*, Archives of Electrical Engineering (2016), DOI: 10.1515/aee-2016-0044.

[17] Tomczuk B., Koteras D., *3D field analysis in 3-phase amorphous modular transformer under increased frequency operation* (2015), DOI: 10.1515/aee-2015-0011.

[18] Łyskawiński W., Sujka P., Szeląg W., Barański M., *Numerical analysis of hysteresis loss in pulse transformer*, Archives of Electrical Engineering (2011), DOI: 10.2478/v10171-011-0018-3.

[19] Pavlovsky M., de Haan S.D., Ferreira J., *Reaching High Power Density in Multikilowatt DC–DC Converters with Galvanic Isolation*, IEEE Transactions on Power Electronics (2009), DOI: 10.1109/TPEL.2008.2008650.

[20] Wilk A., Michna M., *Simulation of the remanence influence on the transient states in a single-phase multiwinding transformer*, Archives of Electrical Engineering (2016), DOI: 66.10.1515/aee-2017-0004.

[21] Wojda R., *Thermal analytical winding size optimization for different conductor shape*, Archives of Electrical Engineering (2015), DOI: 64.10.1515/aee-2015-0017.

[22] Faraji R., Adib E., Farzanehfard H., *Soft-switched non-isolated high step-up multi-port DC-DC converter for hybrid energy system with minimum number of switches*, International Journal of Electrical Power & Energy Systems (2019), DOI: 10.1016/j.ijepes.2018.10.038.

[23] Rodríguez-Lorente A., Barrado A., Calderón C., Fernández C., Lázaro A., *Non-inverting and Non-isolated Magnetically Coupled Buck–Boost Bidirectional DC–DC Converter*, IEEE Transactions on Power Electronics (2020), DOI: 10.1109/TPEL.2020.2984202.

[24] Rodríguez-Lorente A., Barrado A., Calderón C., Fernández C., Lázaro A., *Non-inverting and Non-isolated Magnetically Coupled Buck–Boost Bidirectional DC–DC Converter*, IEEE Transactions on Power Electronics (2020), DOI: 10.1109/TPEL.2020.2984202.

[25] Lyu D., Soeiro T.B., Bauer P., *Impacts of Different Charging Strategies on the Electric Vehicle Battery Charger Circuit Using Phase-Shift Full-Bridge Converter*, IEEE 19th International Power Electronics and Motion Control Conference (PEMC), pp. 256–263 (2021), DOI: 10.1109/PEMC48073.2021.9432497.

[26] Lee I., *Hybrid DC–DC Converter with Phase-Shift or Frequency Modulation for NEV Battery Charger*, IEEE Transactions on Industrial Electronics, vol. 63, no. 2, pp. 884–893 (2016), DOI: 10.1109/TIE.2015.2477345.

[27] Yu W., Lai J.-S., Lai W.–H., Wan H., *Hybrid Resonant and PWM Converter with High Efficiency and Full Soft-Switching Range*, IEEE Transactions on Power Electronics, vol. 27, no. 12, pp. 4925–4933 (2012), DOI: 10.1109/TPEL.2012.2192293.

[28] Liu C., *High-Efficiency Hybrid Full-Bridge–Half-Bridge Converter with Shared ZVS Lagging Leg and Dual Outputs in Series*, IEEE Transactions on Power Electronics, vol. 28, no. 2, pp. 849–861 (2013), DOI: 10.1109/TPEL.2012.2205019.

[29] Fatyga K., Zieliński D., *Comparison of main control strategies for DC/DC stage of bidirectional vehicle charger*, 2017 International Symposium on Electrical Machines (SME), pp. 1–4 (2017), DOI: 10.1109/ISEM.2017.7993585.

[30] Williamson S.S., Rathore A.K., Musavi F., *Industrial Electronics for Electric Transportation: Current State-of-the-Art and Future Challenges*, IEEE Transactions on Industrial Electronics, vol. 62, no. 5, pp. 3021–3032 (2015), DOI: 10.1109/TIE.2015.2409052.

[31] Das P., Pahlevaninezhad M., Drobnik J., Moschopoulos G., Jain P.K., *A Nonlinear Controller Based on a Discrete Energy Function for an AC/DC Boost PFC Converter*, IEEE Transactions on Power Electronics, vol. 28, no. 12, pp. 5458–5476 (2013), DOI: 10.1109/TPEL.2012.2232681.

[32] Barlik R., Nowak M., Grzejszczak P., *Power transfer analysis in a single phase dual active bridge*, Bulletin of the Polish Academy of Sciences: Technical Sciences, vol. 61 (2013), DOI: 10.2478/bpasts-2013-0088.

[33] Brinkel N.G.B., Schram W.L., Alskaif T.A., Lampropoulos I., Ioannis van Sark W.G.J.H.M., *Should we reinforce the grid? Cost and emission optimization of electric vehicle charging under different transformer limits*, Applied Energy, vol. 276, 115285 (2020), DOI: 10.1016/j.apenergy.2020.115285.

[34] Venkata V., Bhajana V., Jarzyna W., Fatyga K., Zieliński D., Kwaśny Ł., *Performance of a SiC MOSFET based isolated dual active bridge DC-DC converter for electro-mobility applications*, Revue Roumaine des Sciences Techniques – Serie Électrotechnique et Énergétique, vol. 64, pp. 383–390 (2020).

[35] Ropoteanu C., Svasta P., Ionescu C., *A study of losses in planar transformers with different layer structure*, IEEE 23rd International Symposium for Design and Technology in Electronic Packaging (SIITME), pp. 255–258 (2017), DOI: 10.1109/SIITME.2017.8259904.

[36] Muhammad Y., *Advanced topologies and modulation schemes for high-efficiency operation of dual-active-bridge series-resonant DC-DC converter* (2018).

[37] Yade O., Gauthier J., Lin-Shi X., Gendrin M., Zaoui A., *Modulation strategy for a Dual Active Bridge converter using Model Predictive Control*, IEEE International Symposium on Predictive Control of Electrical Drives and Power Electronics (2015), DOI: 10.1109/PRECEDE.2015.7395578.

[38] Yan Y., Bai H., Foote A., Wang W., *Securing Full-Power-Range Zero-Voltage Switching in Both Steady-State and Transient Operations for a Dual-Active-Bridge-Based Bidirectional Electric Vehicle Charger*, IEEE Transactions on Power Electronics (2020), DOI: 10.1109/TPEL.2019.2955896.

[39] Jarzyna W., Zielinski D., *The impact of converter's synchronization during FRT voltage recovery in two-phase short circuits*, Selected Problems of Electrical Engineering and Electronics (WZEE), pp. 1–6 (2015), DOI: 10.1109/WZEE.2015.7394043.

[40] Jarzyna W., Zieliński D., Gopakumar K., *An evaluation of the accuracy of inverter sync angle during the grid's disturbances*, Metrology and Measurement Systems, vol. 27, no. 2, pp. 355–371 (2020), DOI: 10.24425/mms.2020.132780.